Structural and biochemical characterization of a novel ZntB (CmaX) transporter protein from Pseudomonas aeruginosa

Stetsenko, Artem; Stehantsev, Pavlo; Dranenko, Natalia O; Gelfand, Mikhail S; Guskov, Albert

Published in:
International Journal of Biological Macromolecules

DOI:
10.1016/j.ijbiomac.2021.06.130

International Journal of Biological Macromolecules 184 (2021) 760–767

Contents lists available at ScienceDirect

International Journal of Biological Macromolecules

journal homepage: www.elsevier.com/locate/ijbiomac

Structural and biochemical characterization of a novel ZntB (CmaX) transporter protein from *Pseudomonas aeruginosa*

Artem Stetsenko [a], Pavlo Stehantsev [a], Natalia O. Dranenko [b], Mikhail S. Gelfand [b,c], Albert Guskov [a,d,*]

[a] *Groningen Biomolecular Sciences and Biotechnology Institute, University of Groningen, the Netherlands*
[b] *Institute for Information Transmission Problems (Kharkevich Institute) RAS, Moscow, Russia*
[c] *Skolkovo Institute of Science and Technology, Moscow, Russia*
[d] *Moscow Institute of Physics and Technology, Dolgoprudny, Russia*

ARTICLE INFO

Keywords:
Membrane proteins
Magnesium transport
CorA proteins
Structural biology

ABSTRACT

The 2-TM-GxN family of membrane proteins is widespread in prokaryotes and plays an important role in transport of divalent cations. The canonical signature motif, which is also a selectivity filter, has a composition of Gly-Met-Asn. Some members though deviate from this composition, however no data are available as to whether this has any functional implications. Here we report the functional and structural analysis of CmaX protein from a pathogenic *Pseudomonas aeruginosa* bacterium, which has a Gly-Ile-Asn signature motif. CmaX readily transports Zn^{2+}, Mg^{2+}, Cd^{2+}, Ni^{2+} and Co^{2+} ions, but it does not utilize proton-symport as does ZntB from *Escherichia coli*. Together with the bioinformatics analysis, our data suggest that deviations from the canonical signature motif do not reveal any changes in substrate selectivity or transport and easily alter in course of evolution.

1. Introduction

The 2-TM-GxN family is responsible for the transport of several divalent cations such as magnesium, zinc, nickel and cobalt ions [1], [2]. This family exists in all domains of life and belongs to Metal Ion Transporters (MIT) superfamily [3]. The current knowledge suggests that all members of the family form pentameric structures (mostly homo-, but there is also evidence for heteropentameric formation [4]), where each monomer consists of two transmembrane α-helices and a large soluble domain. The first long transmembrane helices (TM1) create a protracted pore through which substrate ions flow, and extend all the way into the cytoplasmic domain (Fig. 1). The second transmembrane helices (TM2) arrange into a highly hydrophobic and rigid ring to stabilize the protein in the membrane [5–8]. The loop, connecting TM1 and TM2, contains the signature motif of the family – Gly-X-Asn, where X can be methionine, valine or isoleucine, although in plant homologs of Mrs2 all three amino acids can vary [9–12]. These structural elements – two sets of five helices connected via the loop – are essentially conserved through the family and apparently constitute one of the ancient motifs formed at the earliest stages of evolution for transport.

Contemporary literature has described the 2-TM-GxN family four members – archaeal and bacterial CorAs, protobacterial ZntB, yeast and plant Alr1/2 and eukaryotic Mrs2 [1]. Apart from extensively studied CorA [13], [14], the full-length structure is available only for ZntB from *Escherichia coli* (EcZntB), but its biological function remains vague [13–16]. To investigate further possible roles of ZntB in bacteria, here we have studied ZntB (also annotated as CmaX) from *Pseudomonas aeruginosa* (PaZntB). In contrast to the gene coding EcZntB, the gene coding PaZntB sits in an operon, which additionally includes mechanosensitive ion channel CmpX (MscS type) and a small protein CrfX with an unknown function. This operon is regulated by the extracytoplasmic sigma factors SigX and AlgU, which are involved in regulation of numerous genes involved in cell adaptation, including an outer membrane porin OprF that is crucial for low mass substrate permeability and cell survival [17], [18] among others. It was also shown that the *cmpX* knockout mutation has a large impact on *P. aeruginosa* virulence by increasing sensitivity to antibiotics [19]. This suggests that proteins encoded in *Cmax-CrfX-CmpX* operon play an important role in the life of *P. aeruginosa*, hence we initiated the structural work on these proteins.

In this contribution, we report the cryo-electron microscopy (cryo-EM) full-length structure of PaZntB (CmaX) at an overall resolution of

* Corresponding author at: Groningen Biomolecular Sciences and Biotechnology Institute, University of Groningen, the Netherlands.
E-mail address: a.guskov@rug.nl (A. Guskov).

https://doi.org/10.1016/j.ijbiomac.2021.06.130
Received 21 May 2021; Received in revised form 16 June 2021; Accepted 18 June 2021
Available online 24 June 2021

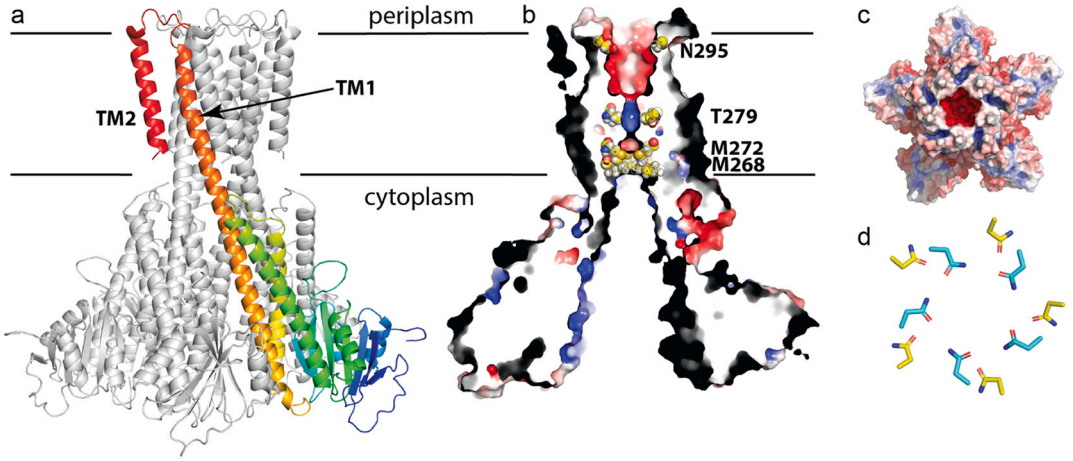

Fig. 1. Structural organization of CmaX (ZntB) from *P. aeruginosa*. (a) Side view, four subunits of pentamer are colored gray, and one is colored rainbow from blue (N-terminus) to red (C-terminus); the approximate position of the membrane is indicated, trans membrane helices 1 and 2 are labeled; (b) the slice through of (a) with the calculated electrostatic potential (±5 kT e^{-1}), residues of the selectivity filter (N295), threonine ring (T279) and the hydrophobic lock (M272 and M268) are shown as spheres and labeled; (c) the view from the periplasm onto (b), note the negative charge at the entry; (d) the comparison of positions of Asn residue of the selectivity filter from EcZntB (cyan) and PaCmaX (PaZntB) (yellow). (For interpretation of the references to color in this figure legend, the reader is referred to the web version of this article.)

Table 1
Data collection and refinement.

Data collection	
Microscope	Titan KRIOS with K3-detector
Voltage	300 kV
Pixel size (Å)	0.656
Micrographs collected (#)	4505
Refinement	
Particles (#)	*243,386*
Resolution (Å; at FSC = 0.143)	*3.03*
CC (model to map fit)	*0.84*
RMS deviations	
Bonds (Å)	0.007
Angles (^{0})	0.77
Chirality (^{0})	0.040
Planarity (^{0})	0.003
Validation	
Clashscore	12.5
Favored rotamers (%)	97
Ramachandran favored (%)	88.31
Ramachandran allowed (%)	11.69
Ramachandran outliers (%)	0

3.03 Å (Table 1, Supplementary Fig. 1) and compare it with the available structures of other members of the 2-TM-GxN family. Additionally, we present the biochemical characterization including fluorescent transport assays and isothermal titration calorimetry measurements. Taken together these results show that PaZntB has an overall same fold as EcZntB and TmCorA, albeit with a different helical arrangement, and is capable to transport Zn^{2+}, Mg^{2+}, Cd^{2+}, Ni^{2+} and Co^{2+} ions, but it seems as if there is no strong proton-coupling as observed with EcZntB.

2. Materials and methods

2.1. Cloning

The gene *cmaX* (NC_002516.2) from *Pseudomonas aeruginosa* PAO1 (strain: PAO1) was codon-optimized for *Escherichia coli* expression and synthesized by GenScript (Piscataway, NJ) and then cloned into a pET-28a (+) plasmid using BamHI and *Eco*RI restriction sites. After the plasmid was mixed with the chemically competent *E. coli* C41 (DE3) cells, transformation was completed by using standard procedures [20].

2.2. Protein expression and membrane vesicle preparation

Expression of ZntB (CmaX) from *Pseudomonas aeruginosa* was performed in a 5-l flask containing 2 l of LB medium (10 g l^{-1} Bacto trypton, 5 g l^{-1} Bacto yeast extract, 10 g l^{-1} NaCl), supplemented with 50 μg ml^{-1} kanamycin. The *E. coli* C41 (DE3) cells with the needed plasmid were grown at 37 °C, 200 rpm to an OD_{600} of 0.6, with an induction by addition of 0.1 mM IPTG. After 3 h of expression the cells were collected by centrifugation (15 min, 7500 *g*, 4 °C), washed in buffer A (50 mM Tris/HCl, pH 8.0) and resuspended in the buffer B (50 mM Tris/HCl, pH 8.0, 250 mM NaCl). Membrane vesicles were either prepared immediately, or the resuspended cells were stored at -80 °C after flash freezing in liquid nitrogen.

Before membrane vesicle preparation, 1 mM $MgSO_4$ and 50–100 μg ml^{-1} DNase were added to the cells. The cells were lysed by high-pressure disruption in High Pressure Homogenizer Type HPL6 (Maximator, Germany), two passages at 25 kPsi for *E. coli* cells, 5 °C and cell debris was removed by low-speed centrifugation (30 min, 12,000 g, 4 °C). Membrane vesicles were collected by ultracentrifugation (120 min, 194,000 g, 4 °C), and resuspended in buffer C (50 mM Tris/HCl, pH 8.0, 250 mM NaCl, 10% glycerol) to a final volume of 1.5 ml per 1 l of cell culture. Subsequently, the membrane vesicles were aliquoted (3 ml per sample), flash frozen in liquid nitrogen and stored at −80 °C.

2.3. Protein purification

Membrane vesicles were thawed rapidly and solubilized in buffer D (50 mM Tris/HCl, pH 8.0, 250 mM NaCl, 1% (w/v) n-dodecyl-β-D-maltopyranoside (DDM, Anatrace)) for 1 h at 4 °C, while gently rocking. DDM was chosen as the most common detergent for membrane protein solubilization [21]. Unsolubilized material was removed by centrifugation (30 min, 194,000 g, 4 °C). The supernatant was incubated for 1 h at 4 °C while gently rocking with Ni^{2+}-sepharose resin (column volume of 0.5 ml), which had been equilibrated with 10 CV of buffer E (50 mM Tris/HCl, pH 8.0, 250 mM NaCl, 50 mM imidazole, 0.02% DDM). Subsequently, the suspension was poured into a 10-ml disposable column (Bio-Rad) and the flow through was collected. The column material was

washed with 10 ml of buffer E. The target protein was eluted in three fractions of buffer F (50 mM Tris/HCl, pH 8.0, 200 mM NaCl, 500 mM imidazole, 0.02% (w/v) DDM) of 200, 750 and 500 μl, respectively. 1 mM of EDTA was added to the second elution fraction to remove co-eluted Ni^{2+} ions and any residual divalent cations. Subsequently, the second elution fraction was purified by size-exclusion chromatography using a Superdex 200 10/300 gel filtration column (GE-Healthcare), equilibrated with buffer G (50 mM Tris/HCl, pH 8.0, 200 mM NaCl, 0.02% (w/v) DDM). After size-exclusion chromatography, the fractions containing the target protein were combined and used directly for the following experiments.

2.4. Reconstitution into proteoliposomes

Reconstitution in proteoliposomes was performed as described [22]. Shortly, polar lipids of *E. coli* and egg phosphatidylcholine (in 3:1 (*w*/w) ratio) were dissolved in chloroform, then dried in a rotary evaporator and subsequently resuspended in buffer containing 50 mM KPi, pH 7.5 to the concentration of 20 mg ml^{-1}. After three freeze-thaw cycles, large unilamellar vesicles (LUVs) were obtained and stored in liquid nitrogen. To prepare proteoliposomes, LUVs were extruded through a 400-nm-diameter polycarbonate filter (Avestin, 11 passages). Obtained liposomes were diluted to 4 mg ml^{-1} in buffer H (50 mM HEPES, pH 7.5) or buffer I (50 mM HEPES, pH 6.5) and subsequently titrated with the increasing Triton X-100 concentration and optical density of the suspension being monitored at 540 nm to cross R_{sat} as described in [22]. The target purified protein was added to the liposomes at a weight ratio of 1:250 (protein/lipid), followed by detergent removal using Bio-beads (50 mg ml^{-1}, four times after 0.5 h, 1 h, 2 h and overnight incubation). Afterwards, proteoliposomes were collected by centrifugation (20 min, 285,775 g, 4 °C) and resuspended in buffer H or buffer I to a lipid concentration of 10 mg ml^{-1} (calculated based on the initial weight). Finally, after three freeze-thaw cycles, obtained proteoliposomes were stored in liquid nitrogen for subsequent experiments.

2.5. Fluorescent transport assays

Zinc, cadmium, nickel and cobalt transport was measured with the Zn^{2+}-sensitive water-soluble fluorophore FluoZin-1 (ThermoFisher, USA). To avoid bleaching of the fluorophore, the sample was shielded from the direct light as much as possible. FluoZin-1 (stock concentration 3 mM in H_2O) was added to a final concentration of 5 μM to the proteoliposomes with desired pH. FluoZin-1 encapsulation was performed by three freeze–thaw cycles and subsequent extrusion through 0.4-μm polycarbonate filters. Extravesicular dye was removed from approximately 500 μl of liposome suspension by size exclusion chromatography on a 2 ml Sephadex G-75 column equilibrated with buffer H or I. Proteoliposomes were collected by ultracentrifugation (25 min, 285,775 g, 4 °C), and the supernatant was removed. Proteoliposomes were resuspended with 10 μl buffer H or I per 2.5 mg of proteoliposomes (protein to lipid ratio 1:250). Transport assays with or without proton gradient were initiated by the addition of 10 mM stock solution of zinc acetate to the desired final concentration. For each measurement, 0.3 mg of proteoliposomes was diluted in 1 ml of desired buffer. A fluorescence time course was measured in a 1 ml cuvette with a stirrer using an excitation wavelength of 490 nm and an emission wavelength of 525 nm. Experiments with empty liposomes were performed in parallel as controls. All measurements were at least triplicated.

For H^+ transport assays, the lumenal buffer of the proteoliposomes was exchanged for buffer J (5 mM HEPES, pH 6.7) by resuspension of the liposomes in this buffer followed by three freeze-thaw cycles and extrusion through 0.4-μm polycarbonate filters. Proteoliposomes were collected by ultracentrifugation (20 min, 285,775 g, 4 °C), and the supernatant was removed. Proteoliposomes were resuspended with 10 μl buffer J per 2.5 mg of proteoliposomes (protein to lipid ratio 1:250). For each measurement, 0.3 mg of proteoliposomes was diluted in 1 ml of buffer K (5 mM HEPES, pH 6.7, 150 nM ACMA). A fluorescence time course was measured in a 1-ml cuvette with a stirrer using an excitation wavelength of 419 nm and an emission wavelength of 483 nm; zinc was added after 3 min of equilibration time. Experiments with empty liposomes were performed in parallel as controls. All measurements were triplicated.

2.6. Isothermal titration calorimetry

Isothermal titration calorimetry experiments were performed with a Nano ITC system (TA Instruments). His-tag was removed with the Pro-Tev Plus (Promega) beforehand. The titrations of various divalent cation salts to PaZntB were performed at 25 °C in 50 mM Tris/HCl, pH 8.0, 250 mM NaCl, 0.02% DDM. The syringe was filled with 0.5-5 mM salts and sequential aliquots of 1.3 μl were added to the sample cell filled with 240 μl 0.03 mM PaZntB. Data were analyzed using the Nano Analyze package (TA Instruments). Error bars represent s.e.m. from three independent measurements.

2.7. Single particle cryo-electron microscopy

The purified ZntB sample (in buffer G) was concentrated to a final concentration of ~10 mg ml^{-1}. Aliquots of 2.7 μl were applied to a freshly glow-discharged holey carbon grids (Quantifoil Cu R1.2/1.3, 200 mesh), excess liquid was blotted for 4–5 s using a FEI Vitrobot Mark IV and the sample was plunge frozen in liquid ethane at a temperature of approximately 100 K. TEM grids were transferred into a Titan Krios 300 keV microscope (FEI, Netherlands), equipped with a K3 direct-electron detector. Zero-loss images were recorded semi-automatically, using the UCSF Image script [23]. The GIF-quantum energy filter was adjusted to a slit width of 20 eV. Images were collected at a nominal magnification of ×130,000 (yielding a pixel size of 1.43 Å) and a defocus range of −1.5 to −3.0 μm. A total of 4505 movie images were collected with 24 frames dose-fractionated over 18 s, in super-resolution counting mode.

Motion correction, CTF estimation, template-based picking, 2D classification, Ab initio volume generation and non-uniform 3D refinement (without symmetry applied if not stated otherwise) were performed using cryoSPARC [24]. Maps were sharpened using Autosharpen Map procedure in Phenix [25]. The sharpened maps were used for the manual model building using Coot [26] and refinement of the coordinates was performed in realspace refine module of Phenix [27], [28]. Visualization and structure interpretation were carried out in UCSF Chimera [29], [30] and PyMol (Schrödinger, LLC). The final model and the map are deposited in PDB and EMDB banks under 7NH9 and EMD-12321.

2.8. Bioinformatics analysis

The phylogenetic tree of CorA/ZntB proteins was constructed using protein sequences from the COG0598 family in the EggNog database [31]. Based on the protein length distribution, the minimum length threshold was set to 233 amino acids to exclude partial proteins (the final set is listed in Suppl. Table 1). The amino acid multiple sequence alignment was constructed by MUSCLE with default parameters [32]. The maximum likelihood phylogenetic tree was constructed using PhyML [33] with the LG model and discrete gamma with four categories; the reliability of internal nodes was estimated using 100 bootstraps. The tree was visualized using IToL [34].

3. Results

3.1. Structure

The structure of PaZntB has a recognizable pentamer arrangement observed so far for all resolved structures of 2-TM-GxN family (Fig. 1).

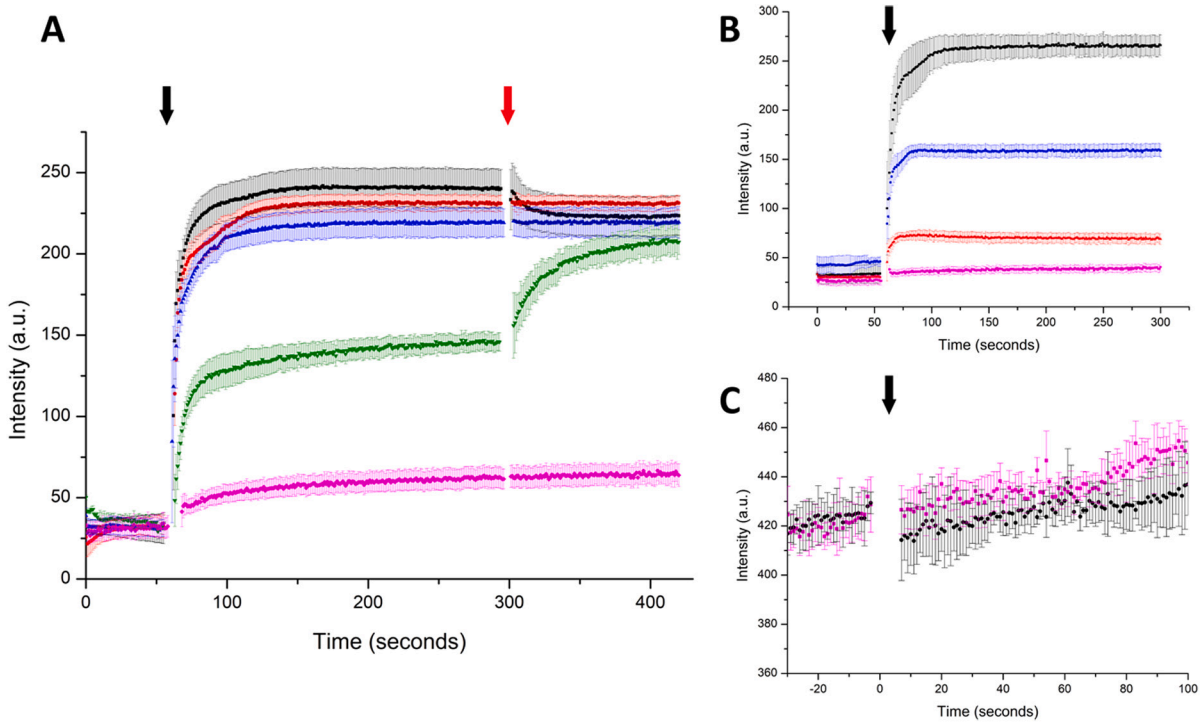

Fig. 2. Fluorescent transport assays (a) of proteoliposomes reconstituted with PaZntB and loaded with fluorescent dye FluoZin-1, 50 μM Zn^{2+} was added at 60 s time point (indicated with a black arrow; color-coded conditions: black — inward pH flux (7.5 in/6.5 out); green — outward pH flux (6.5 in/7.5 out); red and blue — no pH flux at 6.5 and 7.5 pH, magenta — negative control of liposomes without PaZntB with inward pH flux (7.5 in/6.5 out), respectively). FCCP was added at the time point of 300 s (red arrow) to disrupt proton gradients. Error bars represent s.e.m. from more than three technical replicates of independent batches of proteoliposomes. (b) The absence of quenching of the pH-dependent fluorophore ACMA, 50 μM Zn^{2+} was added at 0 s time point (black arrow; black — proteoliposomes with inward and outward 5 mM MOPS, pH 6.7, magenta — negative control of liposomes without PaZntB with inward and outward 5 mM MOPS, pH 6.7. Error bars represent s.e.m. from more than three technical replicates of independent batches of proteoliposomes. (c) Transport of several divalent cations by PaZntB with fluorescent dye FluoZin-1 (black – 50 μM Cd^{2+}, blue – 100 μM Ni^{2+}, red – 200 μM Co^{2+}, magenta – negative control of liposomes without PaZntB with 200 μM Co^{2+}), all ions were added at 60 s time point (black arrow). Error bars represent s.e.m. from more than three technical replicates of independent batches of proteoliposomes. (For interpretation of the references to color in this figure legend, the reader is referred to the web version of this article.)

The cytoplasmic domain consists of seven β-strands arranged in an antiparallel fashion and five α-helices connected to the small transmembrane domain via a long stalk helix. Cytoplasmic domains of PaZntB are nearly identical to those of EcZntB (Cα rmsd 2.2 Å) and similarly have less interactions between protomers compared to TmCorA (Supplementary Fig. 2). Transmembrane domain is formed by the extension of a long cytoplasmic helix 6 into the lipid bilayer (TM1), harbored by TM2 (Fig. 1a).

The TM1 helices form the internal solvent-accessible conical frustum shaped pore, facilitating the movement of charged cations across the lipid bilayer (Fig. 1b). Similarly to EcZntB, this cavity starts from the concave formed by the periplasmic loops, also bearing the family signature motif and the selectivity filter, in this case Gly-Ile-Asn. The lining of the entry is negatively charged (Fig. 1c) hence is attractive for positively charged cations. The pore maintains the negative charge almost entirely through the transmembrane domain with incorporation of some positive charge at Thr279 ring (and this area of positive charge is considerably smaller than observed in EcZntB) and it is tightly sealed about 30 Å below the selectivity filter by the double layered ring formed by Met268 and Met272 sidechains (Fig. 1b), hence resembling architecturally more CorA than ZntB [15]. After the methionine lock (commonly termed hydrophobic lock), the pore leads to the large cytoplasmic cavity which, intriguingly, exclusively maintains positive charge. This is in contrast to EcZntB which has a layer of negative charge followed by layers of positive charge and even more so for TmCorA, which shows preferably negatively charged cavity (Supplementary Fig. 3). However currently it is not clear how these differences in charge distribution precisely affect the transport mechanism.

The most peculiar difference in the transmembrane domain is a position of TM2 helices in PaZntB, which are ~30° tilted in comparison with TM2 helices in EcZntB (Fig. 1; Supplementary Fig. 4). Whether it has any implication to the transport efficiency or protein stability remains to be investigated. Nevertheless, the different arrangement of TM helices leads to the different geometry of the selectivity filter – it is significantly wider than the one in EcZntB (~ 6 Å radius vs 4.5 Å, Fig. 1d). To test whether it impacts the transport and selectivity we conducted thorough biochemical characterizations.

3.2. Transport assays

To characterize the transport of cations via PaZntB, we have performed the fluorescent uptake assays with purified protein reconstituted into liposomes as described previously [16]. The assays with fluorescent dye FluoZin-1, encapsulated into the proteoliposomes, have demonstrated steady uptake of Zn^{2+} ions (Fig. 3a), but significantly smaller influence of proton gradient on zinc transport compared to EcZntB [16]. The level of Zn^{2+} transport in the presence of inward pH gradient (with more basic lumen) is nearly identical to the levels without proton gradient at two different pH values (6.5 and 7.5) (Fig. 2a). It is in stark contrast with EcZntB, where Zn^{2+} uptake is significantly enhanced in the presence of pH gradient [16]. However, quite intriguingly, the uptake of Zn^{2+} ions via PaZntB was noticeably inhibited in the presence of a reverse pH gradient (with more acidic lumen) similarly to EcZntB. To further test the effect of protons on PaZntB we performed additional measurements using pH-sensitive fluorophore 9-amino-6-chloro-2-methoxyacridine (ACMA), however we did not observe the

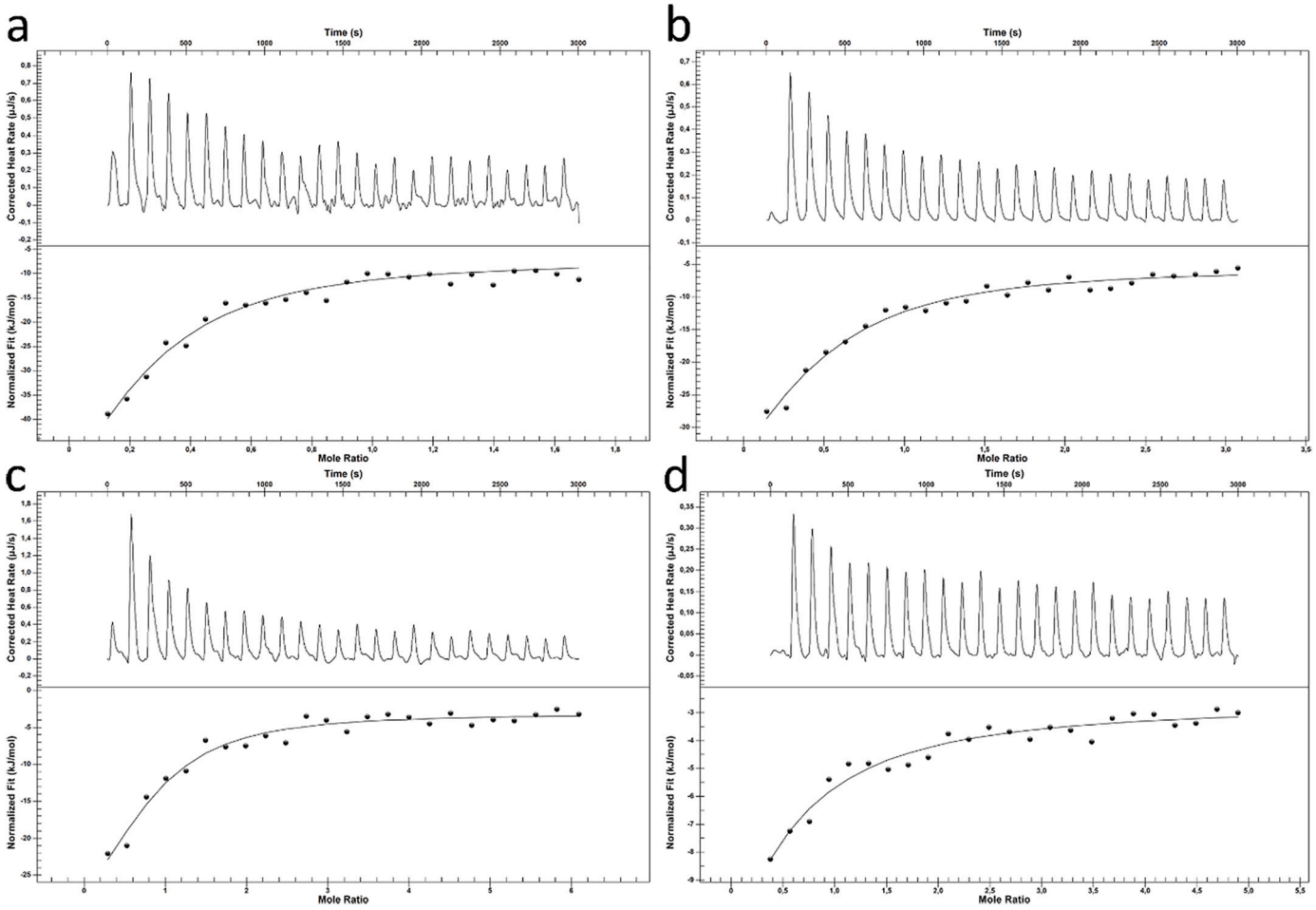

Fig. 3. ITC profiles obtained by titration of (a) Zn^{2+} (b) Cd^{2+} (c) Ni^{2+} (d) Co^{2+} ions to PaZntB.

accumulation of protons inside of the proteoliposomes (Fig. 2b). Finally, we tested PaZntB for other substrates and revealed the comparable transport of Cd^{2+}, Co^{2+} and Ni^{2+} ions (Fig. 2c) as with other studied members of the 2-TM-GxN family, both ZntB and CorA [35].

To characterize the specificity, we additionally performed ITC experiments on His-tag-less protein, which revealed binding of Zn^{2+}, Cd^{2+}, Ni^{2+} and Co^{2+} to PaZntB, with K_d values of 7 ± 2, 12 ± 3, 17 ± 4 and 27 ± 6 μM, respectively, with approximately 0.2 ± 0.1:1 ion:monomer stoichiometry for Zn^{2+} and Cd^{2+} and 1.0 ± 0.2:1 ion:monomer stoichiometry for Co^{2+} and Ni^{2+} (Fig. 3). This different stoichiometry might be indicative of varying preference in the binding sites for cations in PaZntB.

3.3. Comparative genomic analysis

As PaZntB has an atypical selectivity filter, GIN, instead of GMN, we decided to explore how common the deviations from the canonical motif are, therefore we constructed the phylogenetic tree of the proteins with the GxN signature motif. Most proteins with deviations from GMN are located on the branch containing diverse Gammaproteobacteria and Alphaproteobacteria with some Deltaproteobacteria (Fig. 4). The tree topology shows that the protein is actively spreading horizontally between different bacterial species. The following contradictions between the protein tree and the taxonomy indicate likely horizontal transfers: *Salmonella* proteins are found within a branch of *Citrobacter* proteins; a protein from *Cronobacter* is found within a branch of proteins from *Enterobacter*; a group of proteins from *Vibrio* branch close to *Alphaproteobacteria*, best explained by horizontal gene transfer from *Alphaproteobacteria* to the ancestor of *Vibrio* spp. Proteins from *Deltaproteobacteria* are not monophyletic, being observed in the *Alphaproteobacteria* and *Gammaproteobacteria* branches. A protein from *Grimontia* is localized inside the clade of proteins from *Vibrio*. Proteins from *Pseudoalteromonas* with signature motifs GVN and GIN belong to the same clade while the protein with GMN-containing proteins are in a distant branch. Based on the tree structure, we suggest horizontal transfer accompanied with emergence of proteins with the GVN and GIN motifs in genera *Vibrio*, *Oceanicola*, and *Pseudoalterromonas*.

4. Discussion

Pseudomonas aeuroginosa belongs to the *Gammaproteobacteria* phylum and is a common pathogen, responsible for ~1/3 of opportunistic infections in humans [36]. It is characterized by its high adaptability to the environmental changes since it can be found in very different environments such as soil, water, plant and animal tissues. Interestingly, magnesium transport systems have been shown to be of importance for virulence and adaptability of several pathogens [37–39].

The genome of *P. aeruginosa* encodes P-type Mg^{2+} ATPase, Mg^{2+} transporter MgtE, and two members of 2-TM-GxN family, namely CorA and CmaX (termed ZntB in this work). The latter two proteins, despite belonging to the same family, share only ~17% sequence identity. Furthermore, CorA is constitutively expressed house-keeping protein, whereas PaZntB is encoded in an operon together with the small conductance mechanosensitive channel CmpX and the small protein of unknown function CrmX. To check whether PaZntB differs from CorA homologs in terms of functionality and structure we endeavored to

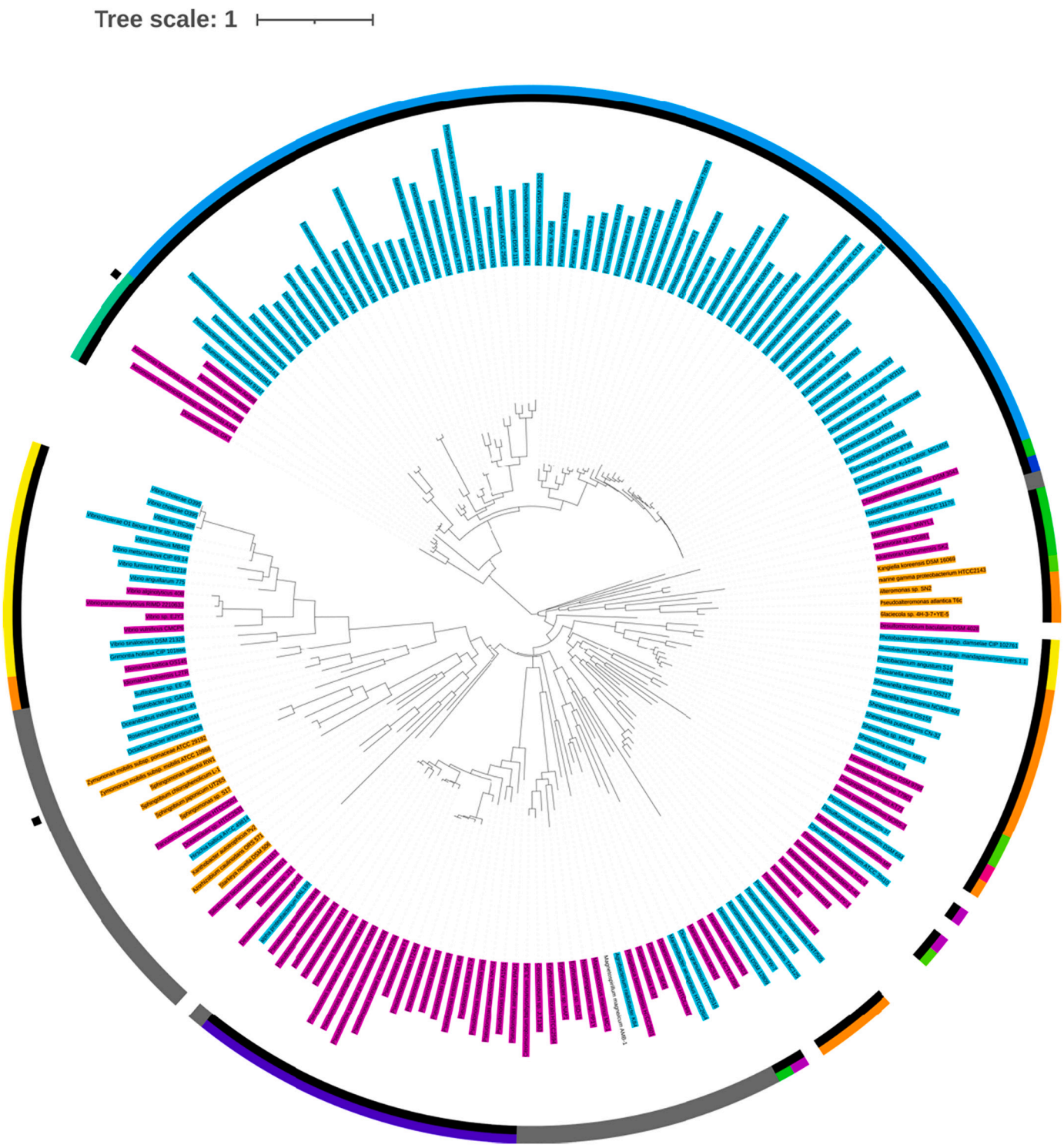

Fig. 4. Branch of the phylogenetic tree containing GxN-motif proteins with deviations from the GMN consensus. Color code is as follows: inner circle – *Gammaproteobacteria* in black, *Alphaproteobacteria* in gray, all other in white, outer circle – nine colors correspond to nine orders of *Gammaproteobacteria*, *Alphaproteobacteria* in gray, all other orders – in white. Two black squares – genes that have binding motifs for zinc repressors in the upstream regions. Protein with motifs: GMN – in orange, GVN – in blue, GIN – in magenta. (For interpretation of the references to color in this figure legend, the reader is referred to the web version of this article.)

characterize it in vitro using transport assays and single particle cryo-EM.

To test for functional differences from known EcZntB and two characterized CorAs, we conducted fluorescence-based transport assays which revealed that both proteins can readily transport Zn^{2+}, Co^{2+}, Ni^{2+} and Cd^{2+} (Fig. 2). Rather unexpectedly, transport of Zn^{2+} is not stimulated by the inward pH gradient (as observed for EcZntB), however it is inhibited with the reverse gradient (Fig. 2a). Nonetheless at the same time we could not detect accumulation of protons (Fig. 2b) within the proteoliposomes during the Zn^{2+} transport. Currently we do not have enough observations to explain such a behavior although it is tempting to speculate that it can be a part of regulatory mechanism to modulate divalent cation flux. Based on the functional and binding assays it seems that the exact composition of the selectivity filter (as well as variations

in pore diameter) play a little role if any. This is corroborated by our bioinformatics analysis that revealed many recent horizontal transfers, in particular from some *Alphaproteoobacteria* to the common ancestors of *Vibrionaceae* (plus *Idiomarina* and some *Alteromonadaceae*) and of *Pseudomonadaceae*. Importantly, there is no detectable correlation of the selectivity filter with phylogeny and functional specificity.

Still the question remains why *P. aeuroginosa* has two highly similar (structurally and functionally) proteins, such as CorA and ZntB. The simplest explanation is that these proteins are redundant and are the result of horizontal gene transfer; however, it does not explain fixation of the transferred gene in the host genome. Another possible explanation is that the functional activity of these proteins depends on the environment and provides fast adaptation to environmental changes. For example, *P. aeuroginosa* might be exposed to extremely different environments during its life cycle, therefore it is tempting to propose that the combination of mechanosensitive channel and ZntB protein might be an intricate safety mechanism to survive the temperature stress [40]. Whereas CmpX might assure the adaptation to the cold temperatures (as was observed for example for MscS in *E.coli* [41]), PaZntB might be involved in adaption to the elevated temperatures [40], as it has been shown recently that its expression is regulated by upstream AlgU extracytoplasmic sigma factor, involved in heat shock response. In general, it is acknowledged that influx of Mg^{2+} can be beneficial for coping with high temperatures as seen from the enhanced expression of magnesium transport systems, such as MgtA, MgtE and CorA (ZntB) leading to the increase in the thermostability (and hence survival) of such pathogens as *Salmonella enterica*, *E. coli* and *P. aeruginosa* [42–44]. Placing the gene into an inducible operon might be a strategy for the better adaption in the organisms exposed to large deviations in the environment. To delineate the contributions of constitutively expressed divalent transporting systems from inducible ones will require a thorough in vivo characterization using knock-out strains.

Supplementary data to this article can be found online at https://doi.org/10.1016/j.ijbiomac.2021.06.130.

CRediT authorship contribution statement

Artem Stetsenko: methodology, investigation, formal analysis, writing – original draft, visualization.

Pavlo Stehantsev: investigation, visualization.

Natalia O. Dranenko: investigation, visualization, software.

Mikhail S. Gelfand: conceptualization, formal analysis, data curation, supervision.

Albert Guskov: conceptualization, validation, formal analysis, writing – review and editing, visualization, supervision, project administration, funding acquisition.

Acknowledgments

We thank Dr. Jan Rheinberger for the help with the preparation of EM grids. The access to NeCEN facilities was funded by the Netherlands Electron Microscopy Infrastructure (NEMI), project number 184.034.014 of the National Roadmap for Large-Scale Research Infrastructure of the Dutch Research Council (NWO). We thank the personnel of NeCEN for the help with data collection. This research was financed by NWO grant 740.018.011 to A.G. Comparative genomic analysis by N. O.D. and M.S.G. was supported by RFBR grant 20-54-14005.

The authors declare no competing interest.

References

[1] V. Knoop, M. Groth-Malonek, M. Gebert, K. Eifler, K. Weyand, Transport of magnesium and other divalent cations: evolution of the 2-TM-GxN proteins in the MIT superfamily, Mol. Gen. Genomics. 274 (3) (2005) 205–216, https://doi.org/10.1007/s00438-005-0011-x.

[2] D. Niegowski, S. Eshaghi, The CorA family: structure and function revisited, Cell. Mol. Life Sci. 64 (19–20) (2007) 2564–2574, https://doi.org/10.1007/s00018-007-7174-z.

[3] S. Prakash, G. Cooper, S. Singhi, M.H. Saier, The ion transporter superfamily, Biochim. Biophys. Acta Biomembr. 1618 (1) (2003) 79–92, https://doi.org/10.1016/j.bbamem.2003.10.010.

[4] M. Herzberg, L. Bauer, A. Kirsten, D.H. Nies, Interplay between seven secondary metal uptake systems is required for full metal resistance of Cupriavidus metallidurans, Metallomics (2016), https://doi.org/10.1039/c5mt00295h.

[5] A. Guskov, S. Eshaghi, The Mechanisms of Mg 2 and Co 2 Transport by the CorA Family of Divalent Cation Transporters vol. 69, Elsevier, 2012.

[6] J. Payandeh, E.F. Pai, A structural basis for Mg2 homeostasis and the CorA translocation cycle, EMBO J. 25 (16) (2006) 3762–3773, https://doi.org/10.1038/sj.emboj.7601269.

[7] S. Eshaghi, D. Niegowski, A. Kohl, D.M. Molina, S.A. Lesley, P. Nordlund, Crystal structure of a divalent metal ion transporter CorA at 2.9 angstrom resolution, Science (80-.) 313 (5785) (2006) 354–357, https://doi.org/10.1126/science.1127121.

[8] R.L. Smith, E. Gottlieb, L.M. Kucharski, M.E. Maguire, Functional similarity between archaeal and bacterial CorA magnesium transporters, J. Bacteriol. 180 (10) (1998) 2788–2791.

[9] S. Ishijima, Z. Shigemi, H. Adachi, N. Makinouchi, I. Sagami, Functional reconstitution and characterization of the Arabidopsis Mg 2 transporter AtMRS2-10 in proteoliposomes, Biochim. Biophys. Acta Biomembr. 1818 (9) (2012) 2202–2208, https://doi.org/10.1016/j.bbamem.2012.04.015.

[10] I. Palombo, D.O. Daley, M. Rapp, Why is the GMN motif conserved in the CorA/Mrs2/Alr1 superfamily of magnesium transport proteins? Biochemistry 52 (28) (2013) 4842–4847, https://doi.org/10.1021/bi4007397.

[11] T. Saito, et al., Expression and functional analysis of the CorA-MRS2-ALR-type magnesium transporter family in rice, Plant Cell Physiol. 54 (10) (2013) 1673–1683, https://doi.org/10.1093/pcp/pct112.

[12] L. Zhang, et al., Molecular identification of the magnesium transport gene family in Brassica napus, Plant Physiol. Biochem. 136 (October) (2019) 204–214, https://doi.org/10.1016/j.plaphy.2019.01.017.

[13] M.E. Maguire, The structure of CorA: a Mg2 -selective channel, Curr. Opin. Struct. Biol. 16 (4) (2006) 432–438, https://doi.org/10.1016/j.sbi.2006.06.006.

[14] N. Nordin, et al., Exploring the structure and function of Thermotoga maritima CorA reveals the mechanism of gating and ion selectivity in Co 2 /Mg 2 transport, Biochem. J. 452 (2) (2015) 367–368, https://doi.org/10.1042/bj4520367.

[15] A. Guskov, et al., Structural insights into the mechanisms of Mg2 uptake, transport, and gating by CorA, Proc. Natl. Acad. Sci. 109 (45) (2012) 18459–18464, https://doi.org/10.1073/pnas.1210076109.

[16] C. Gati, A. Stetsenko, D.J. Slotboom, S.H.W. Scheres, A. Guskov, The structural basis of proton driven zinc transport by ZntB, Nat. Commun. 8 (1) (2017), https://doi.org/10.1038/s41467-017-01483-7.

[17] E. Bouffartigues, et al., Transcription of the oprF gene of pseudomonas aeruginosa is dependent mainly on the sigX sigma factor and is sucrose induced, J. Bacteriol. 194 (16) (2012) 4301–4311, https://doi.org/10.1128/JB.00509-12.

[18] F.S.L. Brinkman, G. Schoofs, R.E.W. Hancock, R. De Mot, Influence of a putative ECF sigma factor on expression of the major outer membrane protein, OprF, in Pseudomonas aeruginosa and Pseudomonas fluorescens, J. Bacteriol. 181 (16) (1999) 4746–4754, https://doi.org/10.1128/jb.181.16.4746-4754.1999.

[19] A.Y. Bhagirath, D. Somayajula, Y. Li, K. Duan, CmpX Affects virulence in Pseudomonas aeruginosa through the Gac/Rsm signaling pathway and by modulating c-di-GMP levels, J. Membr. Biol. 251 (1) (2018) 35–49, https://doi.org/10.1007/s00232-017-9994-6.

[20] H. Inoue, H. Nojima, H. Okayama, High efficiency transformation of Escherichia coli with plasmids, Gene 96 (1) (1990) 23–28, https://doi.org/10.1016/0378-1119(90)90336-P.

[21] A. Stetsenko, A. Guskov, An overview of the top ten detergents used for membrane protein crystallization, Crystals (7) (2017), https://doi.org/10.3390/cryst7070197.

[22] E.R. Geertsma, N.A.B. Nik Mahmood, G.K. Schuurman-Wolters, B. Poolman, Membrane reconstitution of ABC transporters and assays of translocator function, Nat. Protoc. 3 (2) (2008) 256–266, https://doi.org/10.1038/nprot.2007.519.

[23] X. Li, S. Zheng, D.A. Agard, Y. Cheng, Asynchronous data acquisition and on-the-fly analysis of dose fractionated cryoEM images by UCSFImage, J. Struct. Biol. (2015), https://doi.org/10.1016/j.jsb.2015.09.003.

[24] A. Punjani, J.L. Rubinstein, D.J. Fleet, M.A. Brubaker, CryoSPARC: algorithms for rapid unsupervised cryo-EM structure determination, Nat. Methods (2017), https://doi.org/10.1038/nmeth.4169.

[25] T.C. Terwilliger, O.V. Sobolev, P.V. Afonine, P.D. Adams, Automated map sharpening by maximization of detail and connectivity, Acta Crystallogr. Sect. D Struct. Biol. (2018), https://doi.org/10.1107/S2059798318004655.

[26] P. Emsley, B. Lohkamp, W.G. Scott, K. Cowtan, Features and development of Coot, Acta Crystallogr. Sect. D Biol. Crystallogr. (2010), https://doi.org/10.1107/S0907444910007493.

[27] P.V. Afonine, et al., Real-space refinement in PHENIX for cryo-EM and crystallography, Acta Crystallogr. Sect. D Struct. Biol. (2018), https://doi.org/10.1107/S2059798318006551.

[28] P.V. Afonine, et al., New tools for the analysis and validation of cryo-EM maps and atomic models, Acta Crystallogr. Sect. D Struct. Biol. (2018), https://doi.org/10.1107/S2059798318009324.

[29] E.F. Pettersen, et al., UCSF Chimera - a visualization system for exploratory research and analysis, J. Comput. Chem. (2004), https://doi.org/10.1002/jcc.20084.

[30] T.D. Goddard, et al., UCSF ChimeraX: meeting modern challenges in visualization and analysis, Protein Sci. (2018), https://doi.org/10.1002/pro.3235.
[31] J. Huerta-Cepas, et al., EggNOG 5.0: a hierarchical, functionally and phylogenetically annotated orthology resource based on 5090 organisms and 2502 viruses, Nucleic Acids Res. (2019), https://doi.org/10.1093/nar/gky1085.
[32] R.C. Edgar, MUSCLE: multiple sequence alignment with high accuracy and high throughput, Nucleic Acids Res. (2004), https://doi.org/10.1093/nar/gkh340.
[33] S. Guindon, J.F. Dufayard, V. Lefort, M. Anisimova, W. Hordijk, O. Gascuel, New algorithms and methods to estimate maximum-likelihood phylogenies: assessing the performance of PhyML 3.0, Syst. Biol. (2010), https://doi.org/10.1093/sysbio/syq010.
[34] I. Letunic, P. Bork, Interactive tree of Life (iTOL): an online tool for phylogenetic tree display and annotation, Bioinformatics (2007), https://doi.org/10.1093/bioinformatics/btl529.
[35] A. Stetsenko, A. Guskov, Cation permeability in CorA family of proteins, Sci. Rep. 10 (1) (2020) 1–9, https://doi.org/10.1038/s41598-020-57869-z.
[36] G.P. Bodey, R. Bolivar, V. Fainstein, L. Jadeja, Infections caused by Pseudomonas aeruginosa, J. Indiana State Med. Assoc. 5 (2) (1983) 1627–1634.
[37] E.A. Groisman, K. Hollands, M.A. Kriner, E.J. Lee, S.Y. Park, M.H. Pontes, Bacterial Mg2 homeostasis, transport, and virulence, Annu. Rev. Genet. (2013), https://doi.org/10.1146/annurev-genet-051313-051025.
[38] K.M. Papp-Wallace, et al., The CorA Mg2 channel is required for the virulence of Salmonella enterica serovar typhimurium, J. Bacteriol. 190 (19) (2008) 6517–6523, https://doi.org/10.1128/JB.00772-08.
[39] D.C. Ford, G.W.P. Joshua, B.W. Wren, P.C.F. Oyston, The importance of the magnesium transporter MgtB for virulence of Yersinia pseudotuberculosis and Yersinia pestis, Microbiol. (United Kingdom) 160 (2014) 2710–2717, https://doi.org/10.1099/mic.0.080556-0.
[40] E. Bouffartigues, et al., The temperature-regulation of Pseudomonas aeruginosa cmaX-cfrX-cmpX operon reveals an intriguing molecular network ithe sigma fAlgU and SigX, Front. Microbiol. 11 (October) (2020) 1–14, https://doi.org/10.3389/fmicb.2020.579495.
[41] C.A. White-Ziegler, S. Um, N.M. Pérez, A.L. Berns, A.J. Malhowski, S. Young, Low temperature (23 °C) increases expression of biofilm-, cold-shock- and RpoS-dependent genes in Escherichia coli K-12, Microbiology 154 (1) (2008) 148–166, https://doi.org/10.1099/mic.0.2007/012021-0.
[42] K. O'Connor, S.A. Fletcher, L.N. Csonka, Increased expression of Mg2 transport proteins enhances the survival of Salmonella enterica at high temperature, Proc. Natl. Acad. Sci. U. S. A. 106 (41) (2009) 17522–17527, https://doi.org/10.1073/pnas.0906160106.
[43] C.S. Richmond, J.D. Glasner, R. Mau, H. Jin, F.R. Blattner, Genome-wide expression profiling in Escherichia coli K-12, Nucleic Acids Res. 27 (19) (1999) 3821–3835, https://doi.org/10.1093/nar/27.19.3821.
[44] K.G. Chan, K. Priya, C.Y. Chang, A.Y. Abdul Rahman, K.K. Tee, W.F. Yin, Transcriptome analysis of Pseudomonas aeruginosa PAO1 grown at both body and elevated temperatures, PeerJ 2016 (7) (2016) 1–19, https://doi.org/10.7717/peerj.2223.